J|A|C|S
ARTICLES
Published on Web 11/13/2002

# Spin Densities in a Ferromagnetic Bimetallic Chain Compound: Polarized Neutron Diffraction and DFT Calculations

Béatrice Gillon,*,† Corine Mathonière,§ Eliseo Ruiz,‡ Santiago Alvarez,‡ Alain Cousson,† Thekkel M. Rajendiran,§,⊥ and Olivier Kahn§,||

*Laboratoire Léon Brillouin (CEA-CNRS), CEN Saclay, 91191 Gif-sur-Yvette, France, Laboratoire des Sciences Moléculaires, Institut de Chimie de la Matière Condensée de Bordeaux (UPR CNRS No. 9048), 33608, Pessac, France, and Departament de Química Inorgànica, Universitat de Barcelona, Diagonal 647, 08028, Barcelona, Spain*

Received February 7, 2002

***Abstract:*** The spin population distribution in the ferromagnetically coupled hetero-bimetallic chain compound $[MnNi(NO_2)_4(en)_2]$ (en = 1,2-ethanediamine) has been investigated by means of polarized neutron diffraction experiments, and the results compared with those from theoretical estimates obtained via calculations based on density functional theory on dinuclear molecular models of the chain. The spin distributions obtained from experiment and from theory are consistent and reflect a larger spin delocalization from the Ni atom due to the more covalent character of the Ni−N bonds compared to the Mn−O ones. Also a nearly isotropic spin distribution is observed for the more ionic $d^5$ $Mn^{2+}$ ion and a clearly anisotropic distribution for the $d^8$ $Ni^{2+}$ ion. The use of dinuclear molecular models for the calculation of the exchange coupling constant between Ni and Mn provide upper and lower limits (+17.6 and −4.2 $cm^{-1}$) for the experimentally determined value (+1.3 $cm^{-1}$), depending on how the missing part of the chain is simulated, but yield essentially the same spin distribution. The Mn(II)−Ni(II) weak ferromagnetic coupling in the chain is interpreted in a spin delocalization mechanism as resulting from the weakness of the overlap between the magnetic orbitals centered on nickel and those centered on manganese which are only weakly delocalized on the ligands.

## Introduction

The magnetic chain compounds play an important role in the field of molecular magnetism, not only because some of them are among the first molecule-based magnets reported but also because these chain compounds are particularly interesting for one-dimensional physics. A famous example is given by the quasi-one-dimensional $S = 1$ Heisenberg antiferromagnet $[Ni(en)_2(NO_2)]ClO_4$ with en = 1,2-ethanediamine, in which the $NO_2^-$ group acts as a bidentate ligand to two nickel ions, which was obtained in 1982 in Kahn's group, and later investigated by physicists with regard to the existence of a Haldane gap.[1] Very recently, Gatteschi et al. reported the characterization of a radical-bridged Co(II) chain.[2] This compound behaves as a 1D magnetic system, with no occurrence of magnetic ordering down to 2 K. However, it shows magnetic bistability due to slow magnetic relaxation. This phenomenon was known up to now only for molecular clusters and opens new perspectives for magnetic chains as nanowires for information storage devices.[3]

Oxamato-bridged $Mn^{II}Cu^{II}$ chain compounds[4] or radical-bridged Mn(II) compounds[5] are nice examples of molecule-based magnets built on magnetic chains. In $MnCu(pbaOH)(H_2O)_3$ with pbaOH = 2-hydroxy-1,3-propylenebis(oxamato),[4] strong antiferromagnetic interactions take place in the chains and weak antiferromagnetic interactions between the Cu(II) and Mn(II) ions belonging to neighboring chains, leading to ferrimagnetic planes and then to 3D ferrimagnetic ordering below 4.6 K, resulting from magnetic dipolar interactions between the planes. This low temperature is the result of the weakness of interchain interactions. This is the reason the chemists working in this field now pay much attention to the way magnetic chains are connected or prepare directly three-dimensional coordination polymers in order to increase the magnetic ordering temperature.

Recently, we reinvestigated the chemistry of the neutral compound $Ni(en)_2(NO_2)_2$ and obtained a bimetallic chain with

† CEN Saclay.
‡ Universitat de Barcelona.
§ Institut de Chimie de la Matière Condensée de Bordeaux (UPR CNRS No. 9048).
⊥ Permanent address: Department of Chemistry, Pondicherry University, R. V. Nagar, Kalapet, Pondicherry-605 014, India.
|| Deceased on December 8, 1999.

(1) (a) Meyer, A.; Gleizes, A.; Girerd, J. J.; Verdaguer, M.; Kahn, O. *Inorg. Chem.* **1982**, *21*, 1729, (b) Renard J. P.; Verdaguer M.; Regnault L. P.; Erkelens W. A. C.; Rossat-Mignod; Ribas J.; Stirling W. G.; Vettier C. *J. Appl. Phys.* **1988**, *63*, 3538.
(2) Caneschi, A.; Gatteschi, D.; Lalioti, N.; Sangregorio, C.; Sessoli, R.; Venturi, G.; Vindigni, A.; Rettori, A.; Pini, M. G.; Novak, M. A. *Angew. Chem., Int. Ed.* **2001**, *40*, 1760.
(3) Sessoli, R.; Gatteschi, D.; Caneschi, A.; Novak, M. A. *Nature* **1993**, *365*, 141.
(4) (a) Pei, Y.; Verdaguer, M.; Kahn, O.; Sletten, J.; Renard, J.-P. *J. Am. Chem. Soc.* **1986**, *108*, 7428, (b) Kahn, O. *Adv. Inorg. Chem.* **1985**, *43*, 176.
(5) (a) Caneschi, A.; Gatteschi, D.; Renard, J.-P.; Rey, P.; Sessoli, R. *Inorg. Chem.* **1976**, *28*, 1989. (b) Caneschi, A.; Gatteschi, D.; Sessoli, R. *Acc. Chem. Res.* **1989**, *22*, 392.

formula $MnNi(NO_2)_4(en)_2$.[6] The magnetic properties of a polycrystalline sample have been investigated and showed intrachain ferromagnetic interactions, with a long-range antiferromagnetic ordering at 2.4 K. The magnetic data were quantitatively interpreted in the paramagnetic regime, leading to the estimation of the intrachain exchange coupling $J = +1.3$ cm$^{-1}$ (corresponding to the spin Hamiltonian $H = -JS_1 \cdot S_2$ used throughout in this paper). Single-crystal magnetic studies have also been performed to characterize further the antiferromagnetic ordering.[7] The ordered magnetic structure consists of ferromagnetic sheets (formed by parallel chains) stacked up along the *c* direction and antiferromagnetically coupled between them. The compound presents a magnetic anisotropy with an easy axis *c*. A metamagnetic transition is observed to proceed in two steps ($H_{c1}$=1.5 kOe and $H_{c2} = 25$ kOe) for the magnetic field applied along *c*.

In this paper, we propose to analyze the origin of the unusual Mn(II)−Ni(II) ferromagnetic interaction within the chain. In such a $d^5-d^8$ pair, the d orbitals are doubly or singly occupied. Therefore, a positive coupling between Mn(II) and Ni(II) may be obtained with strict orthogonality (or accidental degeneracy) of the magnetic orbitals in the active electron approximation or due to spin polarization effects. The polarized neutron diffraction (PND) technique is a unique tool for clarifying what is the predominant mechanism between the spin delocalization mechanism (and the role of orbital overlap) and the spin polarization mechanism. It gives access to the spin distribution in the cell and enables visualization of the magnetic exchange pathways between the metallic ions through the organic bridge. This technique has been successfully applied to various bimetallic molecular-based compounds presenting either an antiferromagnetic[8−10] or a ferromagnetic coupling[11,12] between the transition metal ions through more or less extended bridges. The text is organized as follows: first the determination of the experimental spin density maps in the $MnNi(NO_2)_4(en)_2$ compound in the paramagnetic state is described. Then density functional theory (DFT) calculations are reported that provide calculated spin populations and the exchange coupling constant for dinuclear models of the chain compound $MnNi(NO_2)_4(en)_2$, and the results are compared with the experimental data.

## Experimental Section and Calculation Methods

**Synthesis.** A 5 mL aliquot of a solution was prepared by mixing methanolic solutions of $Ni(NO_2)_2(en)_2$, $MnCl_2 \cdot 6H_2O$, and $NaNO_2$ following the procedure as described previously.[6] Large crystals (up to 15 mm$^3$) of $MnNi(NO_2)_4(en)_2$ were obtained by aerial diffusion of diethyl oxide into the solution at room temperature.

**Neutron Diffraction Structure Determination at 20 K.** The knowledge of the precise structure of the $MnNi(NO_2)_4(en)_2$ compound at low temperature, including the location of all the hydrogen atoms in the cell, is required for the later polarized neutron data treatment. Therefore, unpolarized neutron diffraction measurements have been collected at 20 K, on the four-circle diffractometer 5C2 of the LLB, at the Orphée reactor, Saclay. The experimental conditions are reported in Table 1 along with the crystallographic data. A crystal of 15 mm$^3$ with the long dimension along the *c* direction was set on the diffractometer and cooled in a helium flux cryostat. The cell parameters determined at 20 K are $a = 14.67(1)$ Å, $b = 7.774(5)$ Å, and $c = 12.40(1)$ Å. The integrated intensities of 3024 reflections were measured, leading to a set of 1917 unique reflections, for which the experimental values of the square of the nuclear structure factors[13] $|F_N(hkl)|^2$ were obtained from the intensities after correction due to the Lorentz geometrical factor. No absorption corrections were applied because of the small value of the linear absorption coefficient estimated to 0.81 cm$^{-1}$. The low-temperature structure has been refined in the conditions described in Table 1, using the least-squares program CRYSTALS.[14] The hydrogen atoms were located with the help of the Fourier difference method. The position parameters and anisotropic thermal parameters were refined for all atoms, and a final weighted reliability factor of 0.043 was obtained, with a goodness of fit equal to 1.02. The extinction was refined but was found to be negligible.

***Table 1.*** Crystallographic Data for the Structure Determination at 20 K

| | |
|---|---|
| **Crystallographic Data** | |
| formula | $C_4H_{16}N_8O_8MnNi$ |
| fw (g·mol$^{-1}$) | 417.87 |
| cryst syst | orthorhombic |
| space group | Pccn |
| color of cryst | pale brownish |
| Z | 4 |
| density (g·cm$^{-3}$) | 1.82 |
| linear absorpn coeff (cm$^{-1}$) for neutrons ($\lambda = 1$ Å) | 0.81 |
| **Data Collection** | |
| diffractometer | 5C2 (Orphée) |
| monochromator | copper |
| wavelength (Å) | 0.83 |
| crystl size (mm$^3$) | 15 |
| *T* (K) | 20 |
| no. of reflcns (cell refinement) | 20 |
| no. of measd reflcns | 3024 |
| no. of unique reflcns | 1917 |
| **Conditions for Refinement and Agreement Factors**[a] | |
| no. of unique reflcns $N_o(F_N > 3\sigma)$ | 791 |
| no. of refined params $N_v$ | 175 |
| $R(F_N)$ | 0.056 |
| $R_w(F_N)$ | 0.043 |
| goodness of fit (GOF) | 1.02 |

[a] $R(F_N) = (\Sigma_{hkl}||F_N^o| - |F_N^c||)/(\Sigma_{hkl}|F_N^o|)$. $R_w(F_N) = [(\Sigma_{hkl}w(|F_N^o| - |F_N^c|)^2)/(\Sigma_{hkl}w|F_N^o|^2)]$. GOF $= [(\Sigma_{hkl}w(|F_N^o| - |F_N^c|)^2)/(N_o - N_c)]^{1/2}$, with $N_o$ = number of reflections, $N_v$ = number of parameters, and $w$ = weighting scheme (Tukey and Price): $w = (1/\sigma)[1 - (\delta F_N/\sigma)^2]^2$.

**Polarized Neutron Diffraction Experiment.** The PND technique[15] enables one to determine the experimental magnetic structure factors which are the Fourier components of the spin density. In the present case, we study the induced spin density in a single crystal in the paramagnetic state (above $T_N$), in which the unpaired electron magnetic moments are aligned by an external magnetic field. The incident neutron polarization is vertical and parallel or antiparallel to the applied magnetic field. The PND technique consists of measuring the ratios *R* between the intensities $I_+$ and $I_-$ diffracted by the sample, without (+) and with reversal (−) of the incident neutron beam polarization. The so-called

(6) Kahn, O.; Bakalbassis, E.; Mathonière, C.; Hagiwara, M.; Katsumata, K.; Ouahab, L. *Inorg. Chem.* **1997**, *36*, 1530.
(7) Feyerherm, R.; Mathonière, C.; Kahn, O. *J. Phys.: Condens. Matter* **2001**, *13*, 2639.
(8) Gillon, B.; Cavata, C.; Schweiss, P.; Journaux, Y.; Kahn, O.; Schneider, D. *J. Am. Chem. Soc.* **1989**, *111*, 7124.
(9) (a) Baron, V.; Gillon, B.; Plantevin, O.; Cousson, A.; Mathonière, C.; Kahn, O.; Grand, A.; Öhrström, L.; Delley, B. *J. Am. Chem. Soc.* **1996**, *118*, 11822, (b) Baron, V.; Gillon, B.; Cousson, A.; Mathonière, C.; Kahn, O.; Grand, A.; Öhrström, L.; Delley, B.; Bonnet, M.; Boucherle, J. X. *J. Am. Chem. Soc.* **1997**, *119*, 3500.
(10) Stride, J. A.; Gillon, B.; Gukasov, A.; Larionova, J.; Clérac, R.; Kahn, O. *C. R. Acad. Sci. Paris* **2001**, *4*, 105.
(11) Aebersold, M.; Gillon, B.; Plantevin, O.; Pardi, L.; Kahn, O.; Bergerat, P.; von Seggern, I.; Tuczek, F.; Öhrström, L.; Grand, A.; Lelièvre-Berna, E. *J. Am. Chem. Soc.* **1998**, *120*, 5238.
(12) Figgis, B. N.; Mason, R.; Smith, A. R. P.; Varghese, J. N.; Williams, G. A. *J. Chem. Soc., Dalton Trans.* **1983**, 703.
(13) The nuclear structure factors are defined by $F_N(\mathbf{K}) = \Sigma_i b_i e^{i\mathbf{K}\mathbf{r}_i} e^{-W_i}$, where i refers to the atoms contained in the unit cell, $b_i$ is the nuclear scattering length characteristic for each chemical element, and $W_i$ is a thermal factor.
(14) Carruthers, J. R.; Watkin, D. J. Betteridge P. W. *CRYSTALS, an Advanced Crystallographic Program System*; University of Oxford: Cambridge, U.K., 1988.
(15) Forsyth, J. B. *At. Energy Rev.* **1979**, *172*, 345.

***Table 2.*** Experimental Data Concerning the Polarized Neutron Measurements

| Experimental Conditions | | |
|---|---|---|
| diffractometer | 5C1(Orphée) | |
| monochromator | Heusler | |
| wavelength (Å) | 0.843 | |
| beam polarization | 0.880(4) | |
| flipping efficiency | 1.000(1) | |
| $T$ (K) | 2.5 | |
| $H$ (T) | 7.0 | |
| **Data Collection** | | |
| vertical axis | c | b |
| crystal size ($mm^3$) | 15 | 15 |
| no. of measd reflcns | 321 | 261 |
| no. of unique reflcns | 121 | 95 |
| no. of unique reflcns with $F_M > \sigma(F_M)$ | 92 | 82 |

flipping ratio $R$ can be written in terms of the magnetic and nuclear structure factors $F_M$ and $F_N$ (which are both real in the case of a centric space group) as

$$R(\mathbf{K}) = \frac{F_N^2 + 2pq^2F_NF_M + q^2F_M^2}{F_N^2 - 2peq^2F_NF_M + q^2F_M^2} \quad (1)$$

where **K** is the scattering vector of the Bragg reflection, $q$ is equal to sin α (α being the angle between the magnetic moments in the sample and the scattering vector), $p$ is the imperfect polarization of the incident beam, and $e$ is the flipping efficiency.

The conditions used for the data collection on the polarized neutron diffractometer 5C1 of the LLB are summarized in Table 2. A preliminary polarized neutron data collection[16] at 4 K with an applied field of 2 T along *c* and then *b* provided surprising results for the spin distribution. To avoid any problem resulting from the magnetic anisotropy[17] when the field is applied along the hard axis *b*,[6] new data were collected at 2.5 K, in the paramagnetic state, just above the magnetic ordering temperature, with an applied field of 7 T in order to ensure the saturation of the magnetization for any orientation of the applied field. The same crystal (15 $mm^3$) as that for the unpolarized experiment has been used for the data collection with the direction *c* vertical. A set of 121 unique *hkl* reflections was obtained with $h_{max} = 14$, $k_{max} = 7$, and $l_{max} = 3$. A second data collection has been performed on another crystal of 15 $mm^3$ oriented with the axis *b* vertical leading to a set of 95 unique reflections for *hkl* reflections with $h_{max} = 13$, $k_{max} = 2$, and $l_{max} = 11$. Only reflections with a sufficiently large nuclear structure factor ($F_N > 4 \times 10^{-12}$ cm) were measured in order to avoid problems with multiple reflections. Only reflections with flipping ratios of $0.25 < R < 4$ were kept in the final data set, leading to 174 reflections for the data treatment, among which 132 were independent.

**Density Functional Theory Calculations.** Theoretical methods can be employed to estimate atomic or orbital spin populations,[18] allowing the comparison with the spin densities detected by characterization techniques, as polarized neutron diffraction[8−9,12,19−20] or nuclear magnetic resonance (NMR). [21−23]

The calculations have been carried out for two molecular models with the Gaussian98 computer code[24] using the hybrid B3LYP method proposed by Becke.[25−27] In previous papers, after evaluating several functionals, we found that the B3LYP method provides very good results for the evaluation of spin populations[18] and of the exchange coupling constants.[28] In all calculations we employed the all-electron double-ζ basis set proposed by Ahlrichs[29] and a triple-ζ basis set with a contraction pattern (842 111/6311/411) for the transition metals.[30] The influence of the inclusion of polarization functions in the main group element basis sets has been also checked.

In the dinuclear molecular model **1**, each missing nearest-neighbor metal atoms of the chain were replaced by a simpler Lewis acid, a proton at 1.4 Å, whereas the rest of the structure was taken from the experimental data. The dinuclear molecular model **2** was taken directly from the crystal structure, except for two bridging nitrito groups that became terminal ligands.

## Description of the Nuclear Structure at 20 K

The main features of the structure previously determined by X-ray diffraction at room temperature[6] remain at low temperature. The interatomic distances, as well as the intra- and interchain distances, at room temperature and at 20 K, are reported in Table 3. The chains become closer to each other with decreasing temperature, while the intrachain distance remains practically unchanged. The structure of the chain at 20 K is displayed in Figure 1. The chain presents a zigzag structure formed by alternating Mn(II) and Ni(II) ions bridged by a $NO_2^-$ group, the oxygen atoms being coordinated to the manganese atom in an $O_2$-chelating mode while the nitrogen atom is bonded to nickel. The nickel ion is located on an inversion center, in a slightly distorted octahedral environment formed by four nitrogen atoms belonging to the two ethanediamine groups and two $NO_2^-$ bridging nitrogen atoms. The manganese ion resides on a 2-fold symmetry axis and presents an unusual coordination sphere constituted by eight oxygen atoms, among which four are at a mean distance of 2.24 Å and four at a slightly larger distance of 2.38 Å (O2, O2′ and O4, O4′). We can describe the manganese coordination polyhedron as a distorted dodecahedron. These eight oxygen atoms originate from four $NO_2^-$ groups surrounding the Mn(II) ion: two bridging and two nonbridging nitro groups. Hydrogen bonding occurs within the chain and between the chains: the shortest hydrogen bonds are reported in Table 4.

## Experimental Spin Density from Polarized Neutron Diffraction

The magnetization density $\rho_m(\mathbf{r})$ is related to the magnetic structure factor with scattering vector **K** through a Fourier


(16) Gillon, B. *Mol. Cryst. Liq. Cryst.* **1999**, *334*, 765.
(17) Schweizer, J. Introduction to Physical Techniques in Molecular Magnetism. In *Proceedings of the Yesa Summer School*; Palacio, F., Ressouche E., Schweizer, J., Eds.; Zaragoza, Spain, 2000.
(18) Cano, J.; Ruiz, E.; Alvarez, S.; Verdaguer, M. *Comments Inorg. Chem.* **1998**, *20*, 27.
(19) Gillon, B.; Schweizer, J. In *Molecules in Physics, Chemistry and Biology*; Maruani, J., Ed.; Kluwer Academic: Dordrecht, The Netherlands, 1989; Vol. 2, pp 111−147.
(20) Figgis, B. N.; Kucharski, E. S.; Vrtis, M. *J. Am. Chem. Soc.* **1993**, *115*, 176.
(21) *NMR of Paramagnetic Molecules*; Berliner, L. J., Reuben, J., Eds.; Plenum Press: New York, 1993.
(22) Bertini, I.; Luchinat, C. *Coord. Chem. Rev.* **1996**, *150*, 29.
(23) La Mar, G. N.; Horrocks, W. DeW., Jr.; Holm, R. H. *NMR of Paramagnetic Molecules*; Academic Press: New York, 1973.
(24) Frisch, M. J.; Trucks, G. W.; Schlegel, H. B.; Scuseria, G. E.; Robb, M. A.; Cheeseman, J. R.; Zakrzewski, V. G.; Montgomery, J. A., Jr.; Stratmann, R. E.; Burant, J. C.; Dapprich, S.; Millam, J. M.; Daniels, A. D.; Kudin, K. N.; Strain, M. C.; Farkas, O.; Tomasi, J.; Barone, V.; Cossi, M.; Cammi, R.; Mennucci, B.; Pomelli, C.; Adamo, C.; Clifford, S.; Ochterski, J.; Petersson, G. A.; Ayala, P. Y.; Cui, Q.; Morokuma, K.; Malick, D. K.; Rabuck, A. D.; Raghavachari, K.; Foresman, J. B.; Cioslowski, J.; Ortiz, J. V.; Stefanov, B. B.; Liu, G.; Liashenko, A.; Piskorz, P.; Komaromi, I.; Gomperts, R.; Martin, R. L.; Fox, D. J.; Keith, T.; Al-Laham, M. A.; Peng, C. Y.; Nanayakkara, A.; Gonzalez, C.; Challacombe, M.; Gill, P. M. W.; Johnson, B. G.; Chen, W.; Wong, M. W.; Andres, J. L.; Head-Gordon, M.; Replogle, E. S.; Pople, J. A. *Gaussian 98*, Revision A.6; Gaussian, Inc.: Pittsburgh, PA, 1998.
(25) Becke, A. D. *J. Chem. Phys.* **1993**, *98*, 5648.
(26) Lee, C.; Yang, W.; Parr, R. G. *Phys. Rev. B* **1988**, *37*, 785.
(27) Becke, A. D. *Phys. Rev. A* **1988**, *38*, 3098.
(28) Ruiz, E.; Alemany, P.; Alvarez, S.; Cano, J. *J. Am. Chem. Soc.* **1997**, *119*, 1297.
(29) Schaefer, A.; Horn, H.; Ahlrichs, R. *J. Chem. Phys.* **1992**, *97*, 2571.
(30) Schaefer, A.; Huber, C.; Ahlrichs, R. *J. Chem. Phys.* **1994**, *100*, 5829.

***Table 3.*** Cell Parameters and Intra- and Intermolecular Distances between Metallic Ions and Interatomic Distances (Å) at 298 and 20 K

| Cell Parameters (Å) | | |
|---|---|---|
| | X-rays ($T$ = 298 K) | neutrons ($T$ = 20K) |
| a | 14.559(2) | 14.67(1) |
| b | 7.898(2) | 7.774(5) |
| c | 12.765(2) | 12.40(1) |

| Intra- and Interchain Distances (Å) | | |
|---|---|---|
| | $T$ = 298 K | $T$ = 20 K |
| Mn···Ni (intrachain) | 4.817(5) | 4.785(3) |
| Mn···Mn (interchain, $c$/2) | 6.382 | 6.20 |

| Interatomic Distances (Å) | | |
|---|---|---|
| | $T$ = 298 K | $T$ = 20 K |
| MnO1 | 2.261(5) | 2.279(7) |
| MnO2 | 2.363(4) | 2.349(5) |
| MnO3 | 2.178(6) | 2.200(6) |
| MnO4 | 2.474(5) | 2.412(6) |
| NiN1 | 2.099(6) | 2.090(3) |
| NiN2 | 2.123(6) | 2.118(2) |
| NiN3 | 2.144(5) | 2.138(3) |
| N3O1 | 1.248(7) | 1.248(5) |
| N3O2 | 1.251(8) | 1.258(5) |
| N1C1 | 1.47(1) | 1.475(4) |
| N2C2 | 1.47(1) | 1.481(5) |
| C1C2 | 1.46(1) | 1.523(6) |
| N4O3 | 1.265(9) | 1.265(5) |
| N4O4 | 1.231(9) | 1.243(6) |

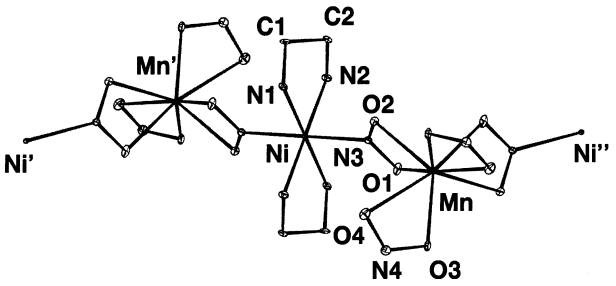


***Figure 1.*** Structure of the chain in $MnNi(NO_2)_4(en)_2$ at 20 K from neutron diffraction. Anisotropic thermal ellipsoids are drawn.

***Table 4.*** Bond Lengths (Å) and Angles (deg) for the Shortest Intra- and Interchain Hydrogen Bonds

| Y–H···X | $d$(H···X) | $d$(Y···X) | (Y–H···X) angle |
|---|---|---|---|
| Intrachain H Bonds | | | |
| N1−H301···O2 | 2.32 | 2.99 | 123 |
| C1−H12···O1 | 2.46 | 3.16 | 120 |
| Interchain H Bonds | | | |
| N2−H102···O3 | 2.24 | 3.19 | 152 |
| N1−H100···O3 | 2.25 | 3.15 | 148 |

transformation:

$$F_M(\mathbf{K}) = \int_{cell} \rho_m(\mathbf{r}) e^{i\mathbf{K}\cdot\mathbf{r}} d\mathbf{r} \qquad (2)$$

The experimental magnetic structure factors $F_M^{exp}$ for the set of measured Bragg reflections are directly deduced from the flipping ratios using eq 1, knowing $F_N$. Therefore the precision obtained on $F_M^{exp}$ depends also on the quality of the structure determination.

The magnetization density is the sum of a pure spin contribution and an orbital contribution. However for most first row transition metals the orbital moment is almost entirely quenched[31] and the orbital contribution can be neglected or treated as a correction.[32] For the reported $Mn^{II}Ni^{II}$ compound, the orbital contribution $F_M^{orb}$ due to the nickel atom has been evaluated[11] with help of the dipolar approximation[32] using the value 2.24(1) for the local Zeeman factor[6] $g_{Ni}$. Moreover, regarding the low-temperature and high-field conditions, a correction $F_{NP}$ due to the polarization of the hydrogen nuclear spins has been taken into account.[33] The pure spin contribution to the magnetic structure factor is then obtained by subtracting these two correcting terms:

$$F_M^{spin} = F_M^{exp} - F_M^{orb} - F_{NP} \qquad (3)$$

The analysis of the PND data consists of refining a model of the spin density by a least-squares procedure[34] on the basis of the magnetic structure factors $F_M^{spin}$. The spin density $\rho(\mathbf{r})$ is assumed to be the sum of atomic densities $\rho_i(\mathbf{r}_i)$ centered on the atoms $i$. Each atomic density is developed over a basis of multipole functions which are products of a Slater-type radial function $R_l^i(r_i)$ and a real spherical harmonic $y_{lm}(\theta_i,\phi_i)$ related to the spherical harmonics $Y_{lm}(\theta_i,\phi_i)$ by $y_{lm+} = (Y_{lm+} + Y_{lm-})/2$ and $y_{lm-} = (Y_{lm+} - Y_{lm-})/2i$. The parameters to be refined are the multipole populations $P_{lm}^i$ and the radial exponents $\zeta_i$.

The model was restricted to the metal ions, the nitro groups, and the nitrogen atoms belonging to the ethanediamine ligands. Spherical densities ($l = 0$, $m = 0$) were assumed for all atoms except nickel. The local octahedral symmetry of the nickel site has been introduced as a constraint on the multipole parameters,[35] in a way similar to that for the previous study of the spin distribution in a $Cu^{II}Ni^{II}$ dinuclear compound.[8]

A reliability factor $R_w(F_M)$ of 0.034 and a goodness of fit (GOF) equal to 1.45 were obtained for the final refinement. A set of 16 parameters was refined for the 174 reflections used. A value of 0.950(5) has been obtained for the scale factor between the two sets of reflections, which confirms that the induced magnetization was practically the same when the field was applied along the $b$ or the $c$ axis. The radial exponents $\zeta$ have been fixed for the nitrogen and oxygen atoms[36] to the respective values of 3.90 and 4.50 $au^{-1}$ and refined for the manganese and nickel atoms, leading to the values 6.82(4) and 9.49(21) $au^{-1}$, respectively. Only the monopole populations $P_{00}$ for the Mn, N, and O atoms have been refined, while, for the nickel atom, the monopole $P_{00}$ and hexadecapole $P_{40}$ populations were refined (with the constraint $P_{44} = 0.7403P_{40}$). The sum of the refined monopole populations $P_{00}$ yields the value of 6.82 $\mu_B$ per MnNi unit for the induced magnetization due to spin only, that is very near saturation. The spin populations given in Table 5 are normalized to 7 $\mu_B$ for each MnNi unit which corresponds to a system of ferromagnetically coupled local spins $S_{Mn^{2+}} = +5/2$ and $S_{Ni^{2+}} = +1$. The corresponding spin density map is represented in Figure 2. In this figure, the spin density is integrated along the direction perpendicular to the NiN3O1O2

(31) Kittel C. *Introduction to Solid State Physics*, 6th ed.; John Wiley & Sons: New York, 1986; p 405.
(32) Squires G. L. *Introduction to the Theory of Thermal Neutron Scattering*; Cambridge University Press: Cambridge, U.K., 1978; p 139.
(33) The structure factors corresponding to the hydrogen nuclear polarization are given by $F_{NP}(\mathbf{K}) = \Sigma_i f_{NP}^i e^{i\mathbf{K}\cdot\mathbf{r}_i} e^{-W_i}$ with $f_{NP}^i = 14.89 \times 10^{-8} H(G)/T(K)$ in $10^{-12}$ cm.
(34) Brown, P. J.; Capiomont, A.; Gillon, B.; Schweizer, J. *J. Magn. Magn. Mater.* **1979**, *14*, 289.
(35) Holladay, A.; Leung, P.; Coppens, P. *Acta Crystallogr.* **1983**, *A39*, 377.
(36) Clementi, E.; Raimondi, D. L. *J. Chem. Phys.* **1963**, *38*, 2686.

***Table 5.*** Experimental and Calculated Spin Populations[a]

| | | DFT calculation s | | | | |
|---|---|---|---|---|---|---|
| | | Mulliken | | NBO | | AIM |
| atom | expt | **1** | **2** | **1** | **2** | **1** |
| Mn | 4.79(2) | +4.79 | +4.83 | +4.73 | +4.77 | +4.61 |
| Ni | 1.64(1) | +1.60 | +1.60 | +1.58 | +1.57 | +1.63 |
| O1 | 0.04(1) | +0.01 | +0.01 | +0.02 | +0.02 | +0.04 |
| O2 | 0.00(1) | +0.01 | +0.01 | +0.02 | +0.02 | +0.04 |
| O3 | 0.04 (2) | −0.02 | +0.01 | +0.01 | +0.02 | +0.05 |
| O4 | 0.01(1) | −0.02 | +0.01 | +0.01 | +0.02 | +0.04 |
| N1 | 0.07(1) | +0.07 | +0.07 | +0.08 | +0.07 | +0.06 |
| N2 | 0.05(2) | +0.07 | +0.07 | +0.08 | +0.07 | +0.06 |
| N3 | 0.07(2) | +0.08 | +0.08 | +0.08 | +0.08 | +0.07 |
| N4 | 0.01 (2) | +0.01 | +0.01 | +0.01 | +0.01 | +0.01 |
| rms | | 0.0009 | 0.0007 | 0.0013 | 0.0009 | 0.0040 |

[a] Experimental spin populations values obtained by multipolar refinement. The final spin population values were normalized to 7 $\mu_B$. Calculated atomic spin populations for dinuclear molecular models **1** and **2** of the chain compound $MnNi(NO_2)_4(en)_2$, obtained with three different population analysis methods and the B3LYP functional (rms is the square mean root deviation relative to the experimental values).

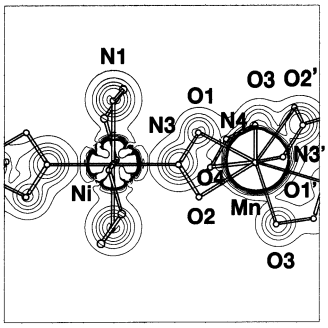


***Figure 2.*** Projection of the induced spin density onto the NiN3O1O2 plane for the ferromagnetic chain compound $MnNi(NO_2)_4(en)_2$ at 2.5 K under an applied field of 7 T. The levels are $\pm 0.005$ e/Å$^2$ with steps of 0.010 e/Å$^2$. Only the low-density levels are drawn.

plane. Only the low-density levels are drawn in order to visualize the spin density delocalization. The spin density is everywhere positive; that indicates that no strong spin polarization effects occur along the chain.

The sum of the populations of the manganese and the eight neighboring oxygen atoms is equal to 4.99(5) $\mu_B$. On the nickel side, the sum of the metal ion population and that of the six surrounding nitrogen atoms amounts to 2.01(3) $\mu_B$. This agrees with the expected spin distribution of alternating moments of 5 and 2 $\mu_B$ along the ferromagnetic MnNi chain. These moments are not strictly localized on the metal ions but are partially delocalized onto the first neighbors. The quantity of spin transferred from the $Mn^{2+}$ ion toward its neighbors only amounts to 4% of the moment associated with the manganese region, while the spin delocalization from $Ni^{2+}$ represents 18% of the total moment on the nickel site. This reflects the stronger covalency of the Ni−N bond compared to that of the Mn−O bond.

The nitrogen atoms surrounding the nickel atom carry similar spin populations, between 0.05(2) and 0.07(2) $\mu_B$. There is no dissymmetry between the bridging and nonbridging ligands contrary to what seemed to indicate the spin distribution obtained from preliminary data collections in different experimental conditions.[16] In the present study, 97% of the magnetic saturation was reached instead of 69% only in the previous collections, for which magnetic anisotropy effects could eventually bias the analysis. However, it must be recalled that such small populations (less than 0.10 $\mu_B$) coming out from multipolar refinement must always be considered with care. The amount of spin transferred from the $Ni^{2+}$ ion toward the nitrogen atom N3 of the bridging $NO_2^-$ group (0.07(2) $\mu_B$), is of the same order of magnitude as that observed in the paramagnetic $Ni(NO_2)_2(ND_3)_4$ compound[37] (0.10(2) $\mu_B$), in which the nickel ion lies in an octahedral environment formed by two $NO_2^-$ groups and four $ND_3$ groups.

The bridging oxygen atoms linked to manganese carry small spin populations, between 0.00(1) and 0.04(1) $\mu_B$, and no significant population is found on the N4 atom of the nonbridging nitro groups. A dissymmetry can be noticed between the spin transfer from the $Mn^{2+}$ ion toward the O1 and O3 atoms in comparison with the O2 and O4 atoms. Larger spin populations are associated with the oxygen atoms O1 and O3, which lie at shorter distances from manganese (2.28 and 2.20 Å) than the oxygen atoms O2 and O4 (2.35 and 2.41 Å). Hydrogen bonding involving these oxygen atoms, as listed in Table 4, could also be responsible for a decrease of the spin population on O2 [38] with respect to O1, but, similarly, the spin population on O3 should be reduced due to the presence of two shorter hydrogen bonds involving O3, which is not the case.

## Density Functional Theory Results

In this theoretical section, the first part will be devoted to the analysis of the atomic spin populations obtained with different theoretical approaches and to the study of the influence of the molecular model chosen, followed by a more detailed analysis of the spin density distribution. In the second part, we will show the results of the calculation of the exchange coupling constant $J$ of $MnNi(NO_2)_4(en)_2$ using molecular models.

**Spin Density Distribution Study.** The theoretical study by means of band theory of a periodic system such as the one studied here is still problematic due to the complexity of the unit cell.[39] Thus, to study the spin density distribution and the exchange coupling for $MnNi(NO_2)_4(en)_2$, we have carried out calculations using two dinuclear molecular models as shown in Figure 3. For the choice of the models the main problem is how to cut the chain; thus, in model **1** we have introduced two protons to simulate the missing neighboring metal atoms, while in model **2** two bridging $NO_2^-$ groups are considered to be terminal ligands.

The spin populations in the high spin state ($S = 7/2$) have been calculated using three different approaches in order to check their agreement with the PND fitted data (see Table 5): the Mulliken population analysis,[40] the natural bond orbital (NBO) population analysis,[41] and the "atoms in molecules" method[42] proposed by Bader using the PROAIM code.[43]

(37) Figgis, B. N.; Reynolds, P. A.; Mason, R. *J. Am. Chem. Soc.* **1983**, *105*, 440.
(38) (a) Pontillon, Y.; Ressouche, E.; Romero, F.; Schweizer, J.; Ziessel, R. *Physica B* **1997**, *234−236*, 788. (b) Gillon, B.; Aebersold, M. A.; Kahn, O.; Pardi, L.; Delley, B. *Chem. Phys.* **1999**, *250*, 23.
(39) Pisani, C. In *Quantum-Mechanical ab-inito Calculation of the Properties of Crystalline Materials*; Pisani, C., Ed.; Springer-Verlag: Berlin, 1996; Vol. 67.
(40) Szabo, A.; Ostlund, N. S. *Modern Quantum Chemistry*; McGraw-Hill: New York, 1989.
(41) Reed, A. E.; Curtiss, L. A.; Weinhold, F. *Chem. Rev.* **1988**, *88*, 899.
(42) Bader, R. F. W. *Atoms in Molecules: A Quantum Theory*; Clarendon: Oxford, U.K., 1994.
(43) PROAIM: Biegler-König, F.; Bader, R. F. W.; Tang, T.-H. *J. Comput. Chem.* **1982**, *13*, 317, modified originally by T. A. Keith and J. R. Cheeseman and by F. Mota to obtain spin populations.

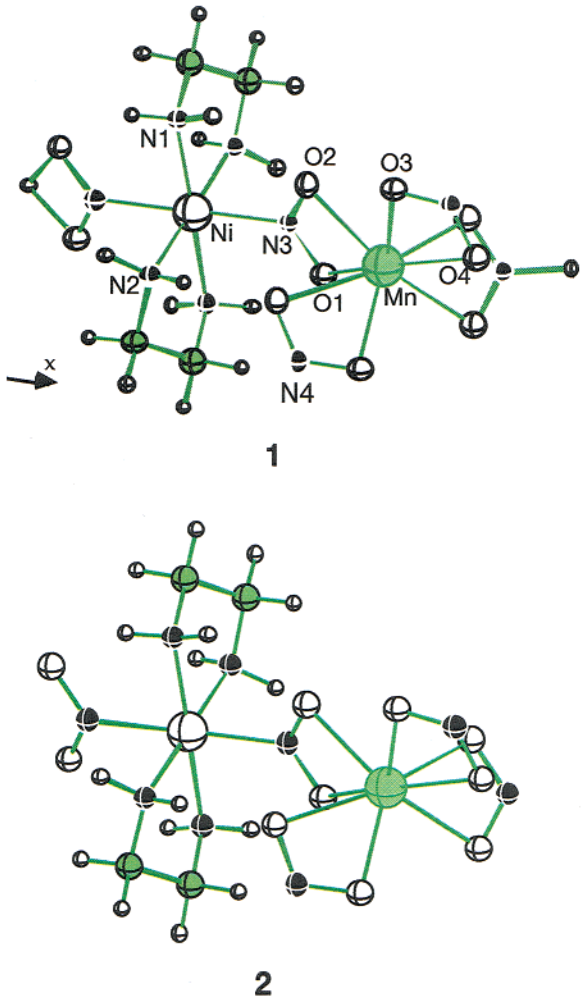


***Figure 3.*** Dinuclear molecular models used for the DFT calculations.

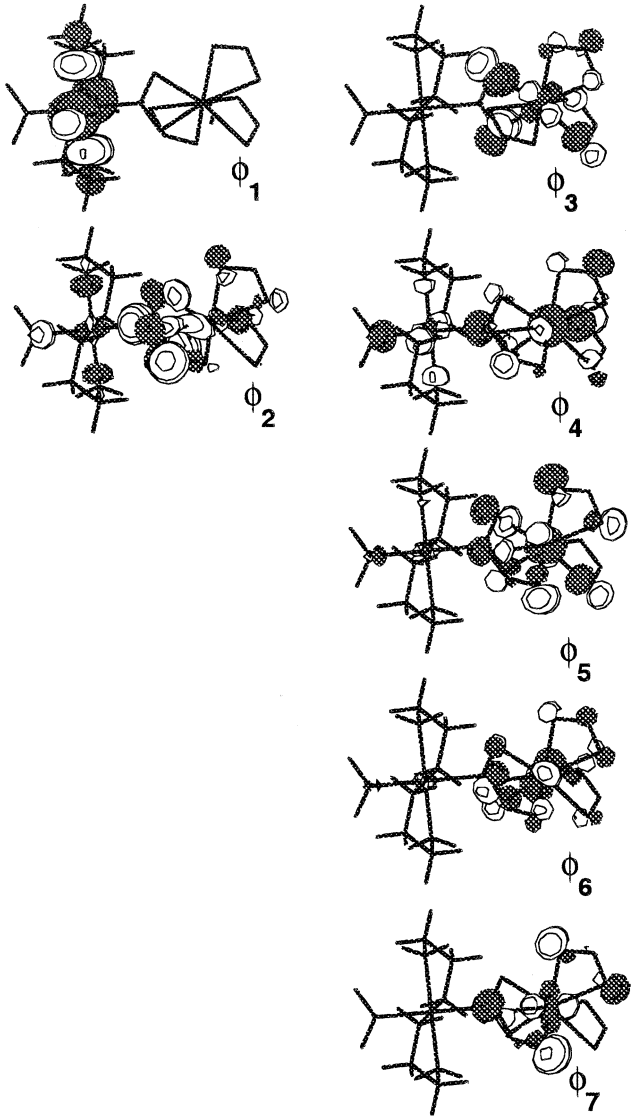


***Figure 4.*** Magnetic orbitals of the ferromagnetic state of model **1**. The orientation of the model is the same as in Figure 3 where the atom labels can be found.

We check first the performance of the different population analysis schemes by comparing with the experimental values. All the results indicate that most of the spin density is localized on the metal atoms. The difference with the number of unpaired electrons indicates the degree of electron delocalization, which is larger for the nickel than for the manganese atom. All the atoms show a positive spin population value except the hydrogen and carbon atoms directly bonded to the nitrogen atoms of the en ligand (not shown). Theoretical and experimental values are in excellent agreement, regardless of the population analysis scheme applied, as indicated by the low root mean square deviation values. Only the Mulliken analysis fails to reproduce the sign of the spin population at O3 and O4 when model **1** is used. The most remarkable difference between the PND and theoretical populations is the dissymmetry between the spin density at O1 and O2, as well as at O3 and O4, found in the PND data.

The results show very small differences between the values for the two models, **1** and **2** (Table 5). The most noticeable effect due to the inclusion of the two hydrogen atoms in **1** is a slightly larger delocalization of the spin population corresponding to the Mn(II) atom. The signs of the calculated spin populations for model **2** are in agreement with the fitted PND values. The increase of the quality of the basis set of the main group elements by introducing polarization functions yields practically identical results (not shown), the largest differences (less than 2%) corresponding to the Ni atom. It is remarkable that even the Mulliken population analysis shows an almost negligible dependence on the basis set despite its well-known drawbacks.[44]

In Figure 4, we show the seven α orbitals, whose equivalent $\beta$ orbitals are empty. In a unrestricted Hartree−Fock scheme, the singly occupied orbitals are those that host the unpaired electrons, not necessarily those with the highest energy. The most salient feature of these orbitals is the negligible contribution at the bridging ligands in most cases, and small exchange integrals should therefore be expected between the d orbitals centered at the Ni and at the Mn atoms. Since, according to Hay, Thibeault, and Hoffman,[45] the ferromagnetic contribution to the exchange coupling constant is associated with the values of such exchange integrals, a weak ferromagnetic coupling should be expected from the magnetic orbital topology, as found in both calculations and experiment. Although two

(44) Jensen, F. *Introduction to Computational Chemistry*; John Wiley & Sons: Chichester, U.K., 1999.
(45) Hay, P. J.; Thibeault, J. C.; Hoffmann, R. *J. Am. Chem. Soc.* **1975**, *97*, 4884.

***Table 6.*** Calculated Orbital Spin Populations with the B3LYP Functional for the Dinuclear Model Compound 1, Obtained with the NBO Population Analysis

| Ni | | Mn | | N3 | | O1 | |
|---|---|---|---|---|---|---|---|
| $e_g$ | 0.77 | 3d | 0.95 | 2s | 0.03 | 2s | 0.00 |
| | 0.72 | | 0.94 | | | | |
| | | | 0.93 | 2p | 0.02 | 2p | 0.02 |
| $t_{2g}$ | 0.00 | | 0.94 | | 0.00 | | 0.00 |
| | 0.02 | | 0.94 | | 0.02 | | 0.00 |
| | 0.08 | | | | | | |
| | | 4s | 0.03 | | | | |
| | | 4p | 0.00 | | | | |
| total | 1.58 | | 4.73 | | 0.08 | | 0.02 |

orbitals ($\phi_2$ and $\phi_4$ in Figure 4) show nonnegligible contributions at the bridges, this is due to the breakdown of the *active electron approximation* due to mixing of the orbitals in Figure 4 with other occupied α orbitals. This interpretation is supported by the analysis of the $\beta$ orbitals, which show no contribution at the bridging atoms, as well as by the negligible spin density calculated for these atoms. We can therefore conclude that the predominant localized nature of the magnetic orbitals is responsible for the ferromagnetic behavior of this compound. The narrow range of energies found for these orbitals is also consistent with the ferromagnetic behavior according to the Hay−Thibeault−Hoffman model.

The analysis of the orbital contributions to the spin populations obtained for model **1** (see Table 6) indicates large values for the $e_g$ orbitals (using the symmetry label corresponding to the octahedral symmetry) of the Ni atom where the unpaired electrons are expected to be. The spin population of the Ni 4s and 4p orbitals is negligible, indicating little mixing with the $e_g$ orbitals. The small positive population in the $t_{2g}$ orbitals should be attributed to spin polarization. The manganese orbital contributions reveal an almost spherical spin population distribution and a small contribution at the 4s orbital that should be attributed to spin polarization.[18] The similar spin populations at the 3d orbital of manganese atom indicate a similar Mn−O bonding character for those orbitals and, consequently, a very small energy difference between them in comparison with manganese atoms adopting, for instance, an octahedral cooordination. The near degeneracy of these 3d orbitals could be responsible for the weakness of the antiferromagnetic contribution to the exchange coupling[45] in agreement with the ferromagnetic behavior experimentally found.

The larger delocalization of the spin density at the nickel atom is clearly reflected in the larger spin population of the nitrogen atoms in comparison with the oxygen atoms coordinated to the manganese. This result is in agreement with the larger degree of covalence of the Ni−N bond compared with the Mn−O one, accounted for by the different electronegativity of nitrogen and oxygen, as well as by the relative position of Ni(II) and Mn(II) in the nephelauxetic series.[46] Consistently, the N1 and N2 atoms present most of their spin density at the 2p orbital oriented toward the nickel atom (+0.06) with a small contribution at the 2s orbital (+0.01).

To learn how the electronic structure of a mononuclear entity is modified upon formation of a dinuclear complex, it is interesting to analyze how the spin populations in our dinuclear

(46) Kettle, S. F. A. *Physical Inorganic Chemistry. A Coordination Chemistry Approach*; Spektrum: Oxford, U.K., 1996.

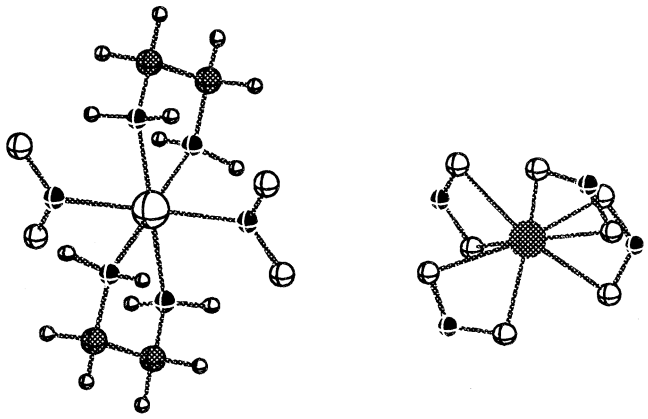

**3** **4**

***Figure 5.*** $[Ni(NO_2)_4(en)_2]$ and $[Mn(NO_2)_4]^{6-}$ mononuclear models used for the DFT calculations.

***Table 7.*** Atomic Spin Populations with the B3LYP Functional for the Molecular Models $[MnNi(NO_2)_4(en)_2]$ (**2**), $[Ni(NO_2)_4(en)_2]$ (**3**), and $[Mn(NO_2)_4]^{6-}$ (**4**) Calculated with the NBO Population Analysis

| atom | **2** | **3** | **4** |
|---|---|---|---|
| Mn | 4.77 | - | 4.78 |
| Ni | 1.57 | 1.57 | - |
| O1 | 0.02 | 0.01 | 0.02 |
| O2 | 0.02 | 0.01 | 0.02 |
| O3 | 0.02 | - | 0.02 |
| O4 | 0.02 | - | 0.02 |
| N1 | 0.07 | 0.07 | - |
| N2 | 0.07 | 0.07 | - |
| N3 | 0.08 | 0.07 | 0.01 |
| N4 | 0.01 | - | 0.01 |

models compare to those in the hypothetical mononuclear parents. Thus, we have calculated the spin population for each metal with its coordinated ligands using the mononuclear models $[Ni(NO_2)_4(en)_2]$ (**3**) and $[Mn(NO_2)_4)]^{6-}$ (**4**) displayed in Figure 5. The calculated spin population is positive at all metal and donor atoms (Table 7), indicating a predominance of spin delocalization over the spin polarization mechanism in the two mononuclear complexes. Furthermore, the atomic spin populations corresponding to the dinuclear complex **2** are practically the sum of those in the two mononuclear entities. Only the $CH_2$ groups of the en ligand show very small negative spin population values (not shown) that can be attributed to spin polarization. The contribution due to spin delocalization from the $Ni^{2+}$ ion toward the oxygen atoms of the $NO_2^-$ bridge is very small (0.01) and so is the contribution due to the $Mn^{2+}$ ion on the bridging nitrogen atom (0.01).

The calculated spin density map, drawn in section in the (Ni, O1, O2) plane in Figure 6, together with the corresponding experimental section, indicates only the presence of regions of positive spin density. The weakness of the polarization mechanism in comparison to the spin delocalization mechanism agrees well with the ferromagnetic coupling found in this compound, since for an even number of atoms in the bridging path the spin alternation due to a spin polarization mechanism would be consistent with an antiferromagnetic ground state.[18]

**Theoretical Evaluation of the Exchange Coupling Constant.** Density functional calculations employing the B3LYP

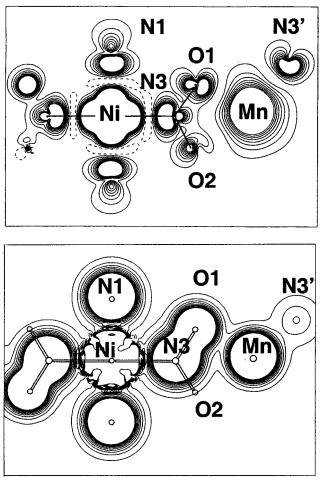


***Figure 6.*** Section of the spin density in the (Ni, O1, O2) plane for the compound $MnNi(NO_2)_4(en)_2$: (top) DFT for model **1**; (bottom) from multipole refinement. The levels are $\pm 0.0005$ e/Å$^3$ with steps of 0.0010 e/Å$^3$. Only the low-density levels are drawn.

functional[25−27] and the broken symmetry approach[47,48] have been successfully applied to the estimation of the exchange coupling constants for a variety of dinuclear complexes, such as alkoxo-,[28] azido-,[49] hydroxo-,[28,50] and oxalato-bridged[51] Cu(II) dinuclear and azido-bridged Ni(II) and Mn(II) complexes.[49] Recently, we have applied the same methodology for the calculation of the exchange coupling constant in heterodinuclear complexes containing an oximato bridging ligand between a Cu(II) center and Ni(II), Mn(II), Mn(III), or Cr(III) atoms with good agreement between computed and experimental values.[52]

The general expression for the calculation of the exchange coupling constant in heterodinuclear systems using methods based on the density functional theory is[53]

$$J = \frac{E_{BS} - E_{HS}}{2S_1S_2 + S_2} \tag{4}$$

where $S_1$ and $S_2$ are the local spins (with $S_2 \leq S_1$), $E_{BS}$ and $E_{HS}$ are the calculated energies of the broken symmetry and high-spin states, respectively. For the particular case of a $Mn^{II}Ni^{II}$ complex ($S_1 = 5/2$ and $S_2 = 1$) broken symmetry and high-spin states are those with with $M_S = 3/2$ and 7/2, respectively. Hence, the following expression results:

$$J = \frac{E_{3/2} - E_{7/2}}{6} \tag{5}$$

Such a formula is not spin-projected and assumes that the energy of the singlet state is adequately simulated by that of the broken symmetry state from density functional calculations, at difference with the criterion adopted by other authors. For a discussion of the relationship between $E_{BS}$ and the energy of the singlet state, the reader is referred to recent papers by us and other authors.[54,55] For more detailed information on computational methodology in this field and on recent applications in transition metal chemistry, the reader is referred to a recent review.[54]

We have calculated $J$ for the two molecular models and obtained values of $+17.6$ and $-4.2$ cm$^{-1}$ for models **1** and **2**, respectively. Notice that a negative value of $J$ indicates that the high-spin state is not the ground state but the spin density remains that of the high-spin state that is positive everywhere. These results are consistent with the very weak coupling revealed by the experimental value[6,7] $J = +1.3$ cm$^{-1}$, since in the chain compound the external nitrito groups are coordinated to a Ni(II) and a Mn(II) ions, which are expected to have an intermediate effect between that of the strong Lewis acid in model **1** ($H^+$) and that of the nonbridging groups. Since the experimental value is very small, what is important rather than theoretically reproducing the numerical value is to find also that the coupling between the two metal atoms is quite weak. Even if both results indicate either ferromagnetic or poor antiferromagnetic coupling, the different values found clearly indicate that the modelization of a chain compound by a dinuclear molecule in the present case introduces significant modifications in the electronic structure and a larger uncertainty in the calculated value of $J$. It is noteworthy that even if the two dinuclear models give different values of $J$, they provide practically the same distribution of the spin population, which is less sensitive to a modification of the molecular structure than the $J$ value.

## Conclusions

The $MnNi(NO_2)_4(en)_2$ compound is the first ferromagnetic bimetallic chain compound for which the structural and magnetic properties have been thoroughly characterized. This paper reports on the determination of the spin distribution along the chain, experimentally with help of polarized neutron diffraction (PND), as well as theoretically with use of density functional theory (DFT).

The main conclusions that can be drawn from the experimental spin density map are the following: The spin density is positive on the whole MnNi dinuclear fragment of the chain that confirms the ferromagnetic nature of the Mn(II)−Ni(II) interaction but also rules out a dominating spin polarization mechanism that would have been responsible for some negative spin density on the bridge. Regions of high positive spin density are observed on the manganese and nickel sites (i.e., considering the metal and donor atoms) corresponding to moments of 4.99(5) $\mu_B$ and 2.01(3) $\mu_B$, in excellent agreement with the idealized spin distribution in a chain of ferromagnetically coupled $S = 5/2$ and $S = 1$ local spins. The spin density is more delocalized on the ligands around nickel than around manganese, reflecting the larger covalency of the Ni−N bond than of the Mn−O bond. The delocalization from the $Ni^{2+}$ ion toward the nitrogen atom of the bridging nitro group is similar to that toward the nitrogen of the ethanediamine groups. A slight dissymmetry can be

(47) Noodleman, L.; Case, D. A. *Adv. Inorg. Chem.* **1992**, *38*, 423.
(48) Noodleman, L.; Peng, C. Y.; Case, D. A.; Mouesca, J. M. *Coord. Chem. Rev.* **1995**, *144*, 199.
(49) Ruiz, E.; Cano, J.; Alvarez, S.; Alemany, P. *J. Am. Chem. Soc.* **1998**, *120*, 11122.
(50) Ruiz, E.; Alemany, P.; Alvarez, S.; Cano, J. *Inorg. Chem.* **1997**, *36*, 3683.
(51) Cano, J.; Alemany, P.; Alvarez, S.; Ruiz, E.; Verdaguer, M. *Chem. Eur. J.* **1998**, *4*, 476.
(52) Cano, J.; Rodríguez-Fortea, A.; Alemany, P.; Alvarez, S.; Ruiz, E. *Chem. Eur. J.* **2000**, *6*, 327.
(53) Ruiz, E.; Cano, J.; Alvarez, S.; Alemany, P. *J. Comput. Chem.* **1999**, *20*, 1391.
(54) Caballol, R.; Castell, O.; Illas, F.; Moreira, I. d. P. R.; Malrieu, J. P. *J. Phys. Chem. A* **1997**, *101*, 7860.
(55) Ruiz, E.; Cano, J.; Alvarez, S.; Alemany, P. *J. Comput. Chem.* **1999**, *20*, 1391. Ruiz, E.; Alvarez, S.; Rodríguez-Fortea, A.; Alemany, P.; Pouillon, Y.; Massobrio, C. In *Magnetism: Molecules to Materials*; Miller, J. S., Drillon, M., Eds.; Wiley-VCH: New York, 2001; Vol. 2, pp 227−279.

noticed on the two oxygen atoms of the $NO_2^-$ bridge. This dissymmetry, if significant, seems to be correlated with the length of the MnO bond. However, it is necessary to be cautious with the small populations associated with the nitrogen and oxygen atoms, which are more sensitive to the refined spin density model than the main spin populations on Mn(II) and Ni(II).

The agreement between the calculated DFT and experimental PND spin distributions is excellent. The main features of the observed spin density in the chain are well-reproduced by DFT calculations on a dinuclear model, except for the dissymmetry between the oxygen populations. The calculations on $[Ni(NO_2)_4(en)_2]$ and $[Mn(NO_2)_4)]^{6-}$ monomers show that the spin distribution in the MnNi entity is the superposition of the two spin distributions of the monomers, with a weak overlap on the bridge. No strong spin polarization contribution is exhibited by the calculations. The ferromagnetic nature of the Mn−Ni coupling can be interpreted in a spin delocalization mechanism, as due to the weakness of the antiferromagnetic contribution to the exchange coupling resulting from the weakness of the overlap between the magnetic orbitals, together with the near degeneracy of the manganese 3d orbitals.

The calculated exchange coupling constant for two dinuclear molecular models of the chain compound provide upper and lower bounds (+17.6 and −4.2 $cm^{-1}$) for the experimental value (+1.3 $cm^{-1}$). These results offer evidence that the modelization of a chain by a dinuclear complex results in a significant degree of uncertainty in the calculated *J* value but suggest that the use of two models in which next-nearest neighbor metal atoms are either omitted or replaced by $H^+$ may give the range of expected values for such systems.

**Acknowledgment.** The authors thank A. Gukasov (LLB) for his help in the low-temperature experiments for the neutron structural study. The theoretical part of this work was supported by DGES (Project PB98-1166-C02-01) and the allocation for computer time at CESCA through a CIRIT grant.

**Supporting Information Available:** Tables of crystal data, structure solution and refinement, atomic coordinates, and anisotropic thermal parameters for $MnNi(NO_2)_4(en)_2$ (PDF). This material is available free of charge via the Internet at http://pubs.acs.org.

JA020188H